

RESEARCH

Open Access



Mibefradil alters intracellular calcium concentration by activation of phospholipase C and IP₃ receptor function

Guilherme H. Souza Bomfim¹ , Erna Mitaishvili¹, Talita Ferreira Aguiar² and Rodrigo S. Lacruz^{1*}

Abstract

Mibefradil is a tetralol derivative originally developed as an antagonist of T-type voltage-gated calcium (Ca²⁺) channels to treat hypertension when used at nanomolar dosage. More recently, its therapeutic application in hypertension has declined and has been instead repurposed as a treatment of cancer cell proliferation and solid tumor growth. Beyond its function as a Ca_v blocker, the micromolar concentration of mibefradil can stimulate a rise in [Ca²⁺]_{cyt} although the mechanism is poorly known. The channel TRPM7 (transient receptor potential melastanin 7), the release of intracellular Ca²⁺ pools, and Ca²⁺ influx by ORAI channels have been associated with the increase in [Ca²⁺]_{cyt} triggered by mibefradil. This study aims to investigate the cellular targets and pathways associated with mibefradil's effect on [Ca²⁺]_{cyt}. To address these questions, we monitored changes in [Ca²⁺]_{cyt} in the specialized mouse epithelial cells (LS8 and ALC) and the widely used HEK-293 cells by stimulating these cells with mibefradil (0.1 μM to 100 μM). We show that mibefradil elicits an increase in [Ca²⁺]_{cyt} at concentrations above 10 μM (IC₅₀ around 50 μM) and a fast Ca²⁺ increase capacity at 100 μM. We found that inhibiting IP₃ receptors, depleting the ER-Ca²⁺ stores, or blocking phospholipase C (PLC), significantly decreased the capacity of mibefradil to elevate [Ca²⁺]_{cyt}. Moreover, the transient application of 100 μM mibefradil triggered Ca²⁺ influx by store-operated Ca²⁺ entry (SOCE) mediated by the ORAI channels. Our findings reveal that IP₃R and PLC are potential new targets of mibefradil offering novel insights into the effects of this drug.

Keywords: Ca²⁺ signaling, Mibefradil, PLC pathway, Ca_v, LS8 cells, ALC cells, HEK293 cells

Introduction

Mibefradil, also known as Ro 40–5967, is an organic compound derivative of tetralol that has been used as a Ca²⁺ channel antagonist (CCA). Patch-clamp studies revealed that mibefradil has an IC₅₀ around 0.3–2.7 μM for Ca²⁺, Na⁺ and K⁺ voltage-dependent currents in HEK-293 cells [1–3]. Mibefradil, a T-type voltage-gated calcium (Ca²⁺) channels (Ca_v 3.1–3.3) inhibitor, was launched by Roche as Posicor® for the treatment of hypertension and stable angina at doses containing 50–100 mg once a day [1, 4]. The maximum plasma

circulating levels of mibefradil were around 1 μg/mL after 1–2 h of the single 100 mg dose [4, 5]. Although mibefradil has a potent effect on T-type CCA, being 10- to 30-fold higher for T-type than L-type [4], adverse clinical outcomes resulted in its withdrawal from the market in 1998 because of drug-drug interactions, side-effects, and inhibition of cytochrome P450 3A4 [6].

Recently, mibefradil has seen a renewed pharmacological interest being an FDA “orphan drug” approved for its efficacy in cancer management [6–8]. Mibefradil has been used to treat ovarian and pancreatic cancer, glioblastoma and has an anti-proliferative effect on several cancer cell lines [8–13]. In melanoma cells, the anti-proliferative and anti-tumoral properties of mibefradil were dependent on caspase activation, the transfer of Ca²⁺

* Correspondence: rodrigo.lacruz@nyu.edu; rs10@nyu.edu

¹Department of Molecular Pathobiology, New York University College of Dentistry, New York, NY 10010, USA
Full list of author information is available at the end of the article

into the endoplasmic reticulum (ER) [14, 15], and the inhibition of basal macroautophagy which is constitutively active in melanoma cells [16]. In addition, retinoblastoma and glioma cells exposed to micromolar concentrations ($\geq 10 \mu\text{M}$) of mibefradil revealed an increase in the number of cells in the G1 phase and a decrease in the number of cells in the S-phase in a dose-dependent manner [12, 17].

From the pharmacological viewpoint, *in vitro* studies show that the use of mibefradil at micromolar concentrations (10–100 μM) elicits an increase in $[\text{Ca}^{2+}]_{\text{cyt}}$ although the molecular mechanism involved is unclear [18–20]. Possibilities include a slow recovery from the opening of the Ca_v block [21] or the activation of the Mg^{2+} channel TRPM7 (transient receptor potential melastatin 7) that is permeable to Ca^{2+} [20]. In HEK-293 cells overexpressing TRPM7 channels, mibefradil (100 μM) increased $[\text{Ca}^{2+}]_{\text{cyt}}$ that was abolished by perfusing with the TRPM7 antagonist NS8593 [20]. Another potential contributor associated with the elevation in $[\text{Ca}^{2+}]_{\text{cyt}}$ elicited by mibefradil is the release of Ca^{2+} from intracellular stores [18] mediated by the activation of inositol 1,4,5-triphosphate (IP_3) receptors (IP_3R) [19].

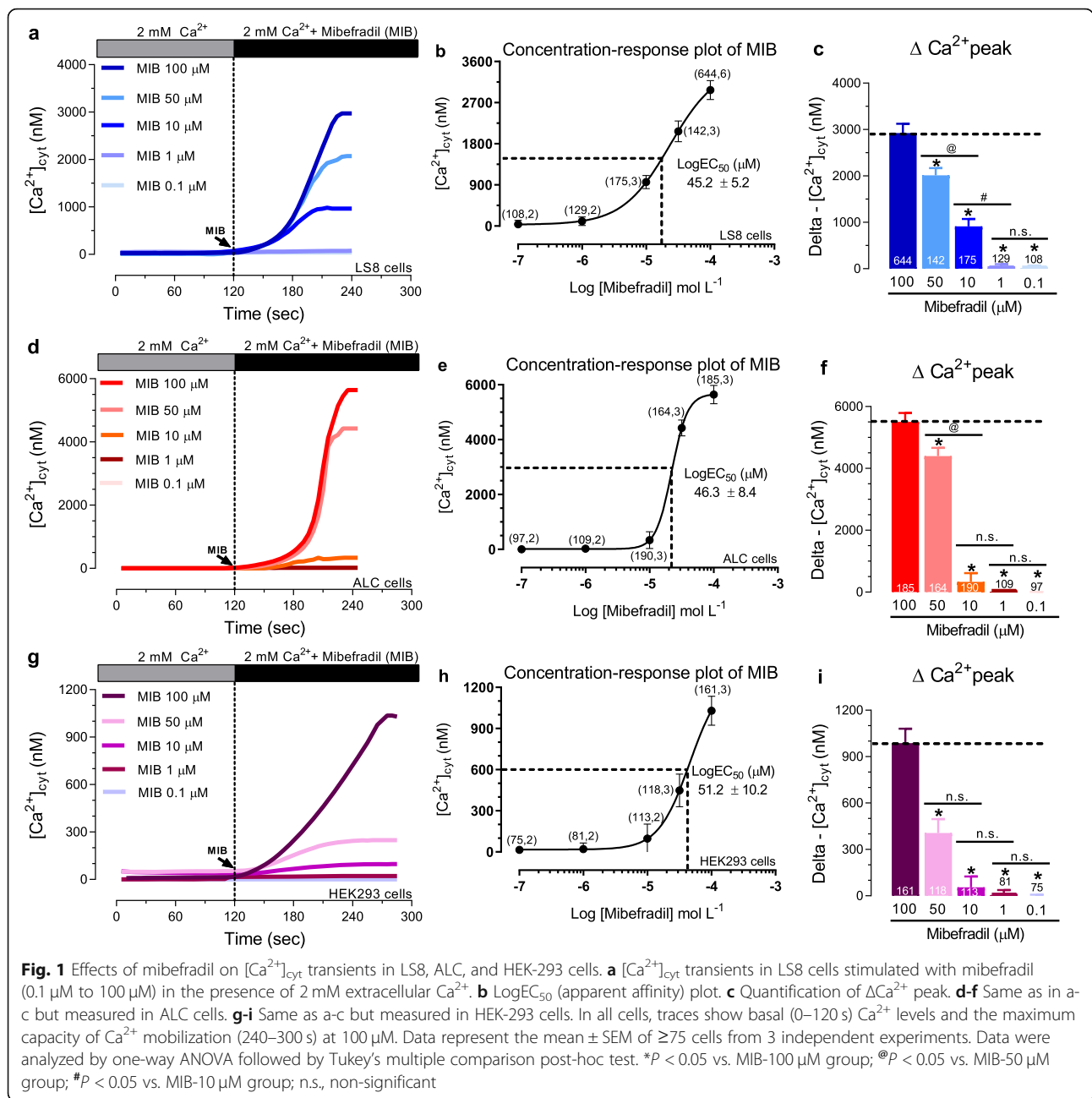
Physiologically, the release of Ca^{2+} pools from the endoplasmic reticulum (ER) is generated through a family of G protein-coupled (GPCRs) and/or enzyme-linked receptors at the cell membrane in response to an agonist activating primary (β - γ) and/or secondary (δ) phospholipases C (PLC) isozymes, a group of Ca^{2+} -dependent phosphodiesterases hydrolyzing phosphatidyl-inositol bisphosphate (PIP_2) into 1,2-diacylglycerol (DAG) and (IP_3) [22]. DAG and/or cell depolarization elicits Ca^{2+} influx through of the functional L-type Ca_v 1.2 and T-type Ca_v 3.1–3.3 [22, 23]. The binding of IP_3 to its receptors in the ER membrane releases Ca^{2+} pools via the IP_3R channels subtype 1, 2, and 3 [23]. This step stimulates Ca^{2+} uptake from extracellular sources via the store-operated Ca^{2+} entry (SOCE) pathway that is mediated by the Ca^{2+} -release-activated Ca^{2+} (CRAC) channel components STIM1/2 and ORAI1–3, replenishing the ER Ca^{2+} stores and activating Ca^{2+} -dependent pathways [24]. Electrophysiological studies reported that mibefradil blocked CRAC currents in a concentration-dependent manner (10–100 μM) in HEK-293 cells overexpressing STIM-ORAI1–3 [25]. This may suggest an interaction with the ORAI channels when acutely perfused. Pretreatment with mibefradil (100 μM) for 24 h abolished ER- Ca^{2+} release and Ca^{2+} influx [25]. Additionally, Johnson et al. demonstrated that 20 μM mibefradil increases $[\text{Ca}^{2+}]_{\text{cyt}}$ via STIM1 and ORAI-1 [26]. Thus, addressing the effects of mibefradil in $[\text{Ca}^{2+}]_{\text{cyt}}$ and its impact on the CRAC channels is important to better understand the broader biological effects of this drug.

Here, we have investigated the cellular targets and pathways associated with the transient application of mibefradil and its effect on $[\text{Ca}^{2+}]_{\text{cyt}}$ *in vitro*. Using the murine epithelial cells LS8 and ALC, and the human HEK-293 cells that are a generalized cell model widely used in signal transduction research [27], we show that mibefradil (0.1 μM to 100 μM) elicited a significant increase in $[\text{Ca}^{2+}]_{\text{cyt}}$ in all cell lines. We found that this effect was reduced or abolished by inhibiting IP_3R or PLC, or by depleting the ER- Ca^{2+} stores. Mibefradil also triggered SOCE, likely as a result of its role in activating the PLC pathway. Taken together, our findings suggest that the application of mibefradil at micromolar ($\geq 10 \mu\text{M}$) concentrations elevates $[\text{Ca}^{2+}]_{\text{cyt}}$, highlighting its effects on the PLC pathway and the ER- Ca^{2+} released via the IP_3R as potential targets thus providing novel insights into the effects of mibefradil.

Results

Mibefradil caused a concentration-dependent increase in $[\text{Ca}^{2+}]_{\text{cyt}}$

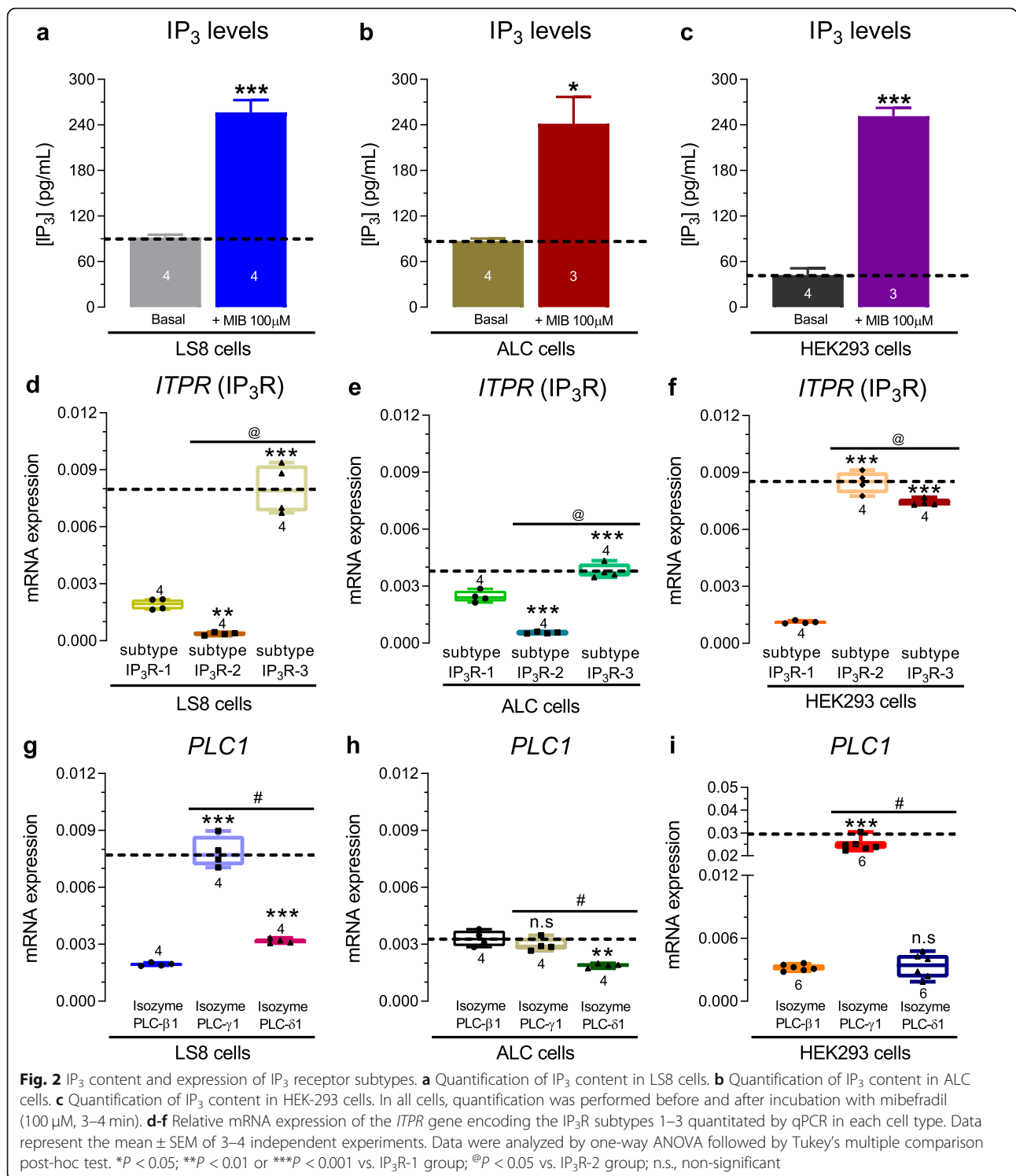
To determine the maximum capacity of Ca^{2+} mobilization by mibefradil, we constructed concentration-effect curves (0.1–100 μM) in murine LS8 and ALC and in human HEK-293 cell lines (Fig. 1). In an extracellular 2 mM Ca^{2+} solution, the perfusion of 0.1–1 μM mibefradil, commonly used to block Ca_v 1.2–3.3 [4], had no effect in $[\text{Ca}^{2+}]_{\text{cyt}}$ in any of the cell lines. By contrast, at concentrations above 10 μM , mibefradil raised $[\text{Ca}^{2+}]_{\text{cyt}}$ from nanomolar to micromolar (~ 1 –5 μM) levels, with a maximum Ca^{2+} increase at 100 μM (Fig. 1). No background autofluorescence was detected in the Ringer's solution with or without mibefradil (50 μM , 100 μM) (Fig. S1). Although LS8, ALC, and HEK-293 cells showed differences in the maximum capacity of Ca^{2+} transients, they all revealed similar values of LogEC_{50} (~ 45 –51 μM) (Fig. 1b, e, h). The efficiency of mibefradil to elevate $[\text{Ca}^{2+}]_{\text{cyt}}$ is demonstrated by a loss of the signal when mibefradil is removed from the solutions (Fig. S2). To ascertain if TRPM7 channels are a potential target of mibefradil, we used the selective TRPM7 agonist naltriben (100 μM) [28]. Under resting extracellular Ca^{2+} levels (2 mM Ca^{2+}), naltriben stimulation did not elicit an increase in $[\text{Ca}^{2+}]_{\text{cyt}}$ in LS8 and ALC cells, although it caused a small elevation (~ 30 nM) in HEK-293 cells (Fig. S3). Taken together, these data suggest that TRPM7 channels are not the main target of mibefradil although these channels may have a small contribution. Our results, together with previous reports [18–20, 29], showed that mibefradil stimulates an increase in $[\text{Ca}^{2+}]_{\text{cyt}}$ when used above 10 μM , with a maximum $[\text{Ca}^{2+}]_{\text{cyt}}$ increase at 100 μM . Thus, we used 100 μM mibefradil to study its effects on Ca^{2+} transients and possible molecular targets.



IP₃ levels and expression and inhibition of IP₃ receptors

To address the effects of mibefradil on IP₃ signaling we first investigated if mibefradil affected the IP₃ content in cells. We lysed cells (1.10⁶ cells/mL) of each type to measure the IP₃ levels before and after mibefradil stimulation (100 μ M for 3–4 min) (Fig. 2). Under basal conditions, the IP₃ content was 91 \pm 3.8 pg/ml in LS8, 87 \pm 3.4 pg/ml in ALC, and 43 \pm 8.7 pg/ml in HEK-293 cells. After mibefradil stimulation, the IP₃ content was ~2-fold higher in LS8 and ALC cells and ~6-fold higher in HEK-293 cells (Fig. 2a-c). We also investigated IP₃R expression and function. The IP₃R

subtype 3 gene (*ITPR3*) was the most highly expressed in LS8 and ALC cells but type 2 (*ITPR2*) was the most abundant mRNA in HEK-293 cells (Fig. 2d-f). To address the functional contribution of IP₃R_s under mibefradil stimulation, we pretreated the cells with the membrane-permeable IP₃R inhibitor Xestospongine C (3 μ M, for 20 min) [30, 31] in a Ca^{2+} -free Ringer's solution. Xestospongine C drastically reduced the ΔCa^{2+} peak in LS8 (~85%), ALC (~70%), and HEK-293 (~60%) cells (Fig. 3b, e, h). This IP₃R inhibitor also caused a slowdown in the Ca^{2+} influx rate in LS8 and ALC cells (Fig. 3c, f). These results, together with the IP₃ content data, suggest that the rise in



[Ca²⁺]_{cyt} elicited by mibefradil (100 µM) involves modulation of IP₃ and IP₃R.

ER-Ca²⁺ depletion impacts the effects of mibefradil

Next, to address the role of the largest intracellular Ca²⁺ store, the ER, we passively depleted the ER Ca²⁺ content

with the reversible SERCA inhibitor CPA (cyclopiazonic acid, 20 µM), prior to stimulating the LS8, ALC and HEK-293 cells with mibefradil in a Ca²⁺-free Ringer's solution (Fig. 3j). CPA triggered a rise in [Ca²⁺]_{cyt} ~ 200–400 nM (Fig. 3j-k) in all cells. After ER-Ca²⁺ depletion, mibefradil (100 µM) perfusion had no effect in

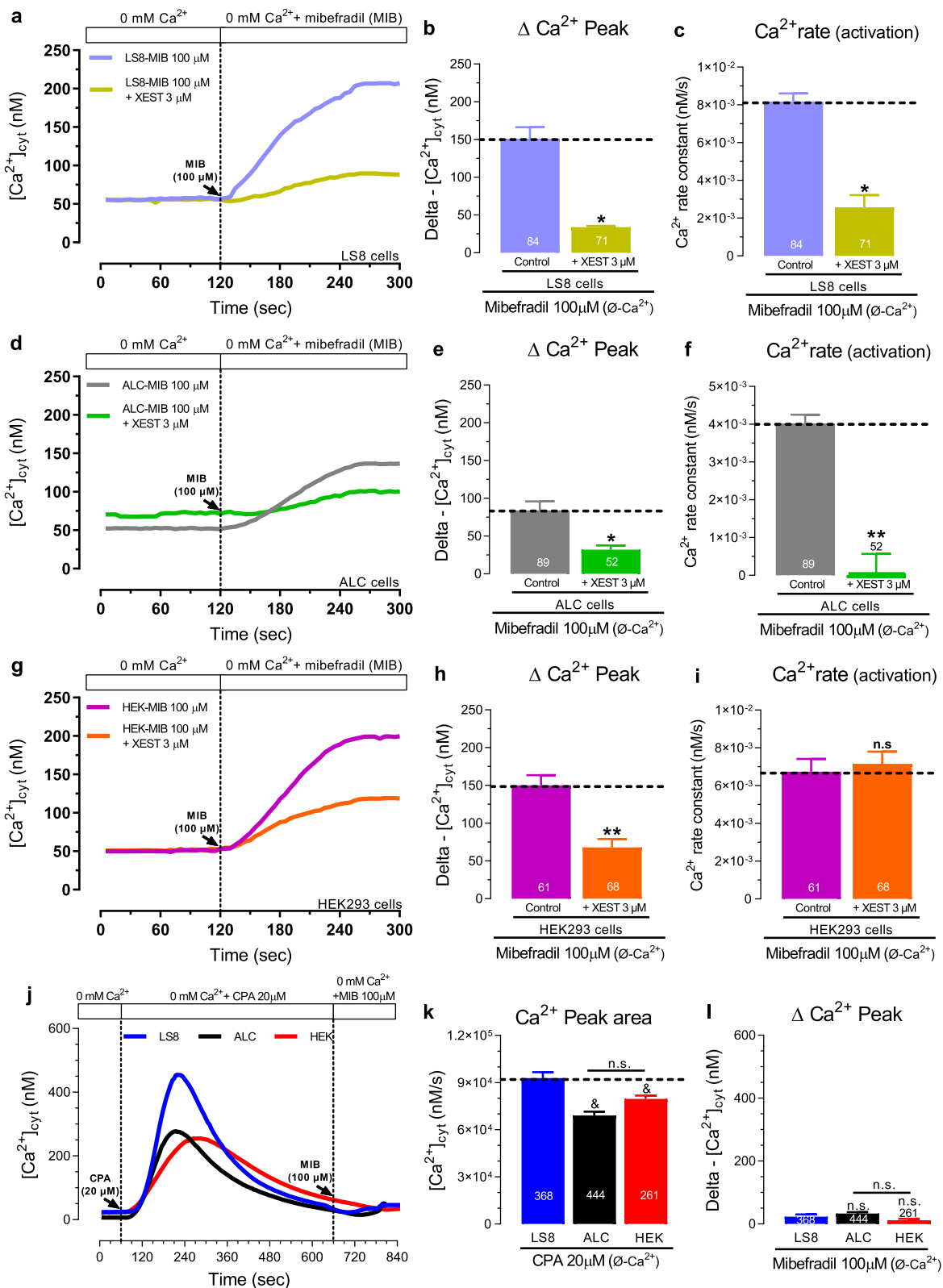


Fig. 3 (See legend on next page.)

(See figure on previous page.)

Fig. 3 Effects of mibefradil are reduced or abolished by IP₃ R antagonist and ER-Ca²⁺ depletion. **a** Original traces of [Ca²⁺]_{cyt} transients in Xestospongine C treated LS8 cells in Ca²⁺-free Ringer's solution before and after mibefradil (100 μM) stimulation. **b** Quantification of the Δ Ca²⁺ peak. **c** Quantification of the Ca²⁺ influx rate. **d-f** Same as in a-c but in ALC cells. **g-i** Same as in a-c but in HEK-293 cells. **j** Original traces of [Ca²⁺]_{cyt} transients in CPA stimulated LS8, ALC, and HEK-293 cells in Ca²⁺-free Ringer's solution followed by the application of mibefradil (100 μM). **k** Quantification of the Δ Ca²⁺ peak under CPA stimulation. **l** Quantification of the Δ Ca²⁺ peak under mibefradil stimulation. Data represent the mean ± SEM of ≥52 cells from 3 independent experiments. Data were analyzed by two-tailed unpaired Student's t-test. **P* < 0.05 or ****P* < 0.01 vs. respective MIB-100 μM (control) group; n.s., non-significant. In ER-Ca²⁺ depletion experiments elicited by CPA (20 μM), the data were analyzed by one-way ANOVA followed by Tukey's multiple comparison post-hoc test. [§]*P* < 0.05 vs. LS8 group n.s., non-significant

rising [Ca²⁺]_{cyt} (Fig. 3l). Similar results were observed when ER-Ca²⁺ depletion was elicited by stimulation with ATP prior to the application of mibefradil in a Ca²⁺-free Ringer's solution, as shown in the ALC cells (Fig. S4). These results suggest that ER-Ca²⁺ stores are an important contributor to the effects of mibefradil.

PLC function is modulated by mibefradil

We first addressed the gene expression levels of the primary (β-γ) and secondary (δ) PLC isoforms. We found that the mRNA encoding PLC-γ1 was the most highly expressed in LS8 and HEK-293 cells, whereas in ALC cells, the β-γ isoforms were dominant (Fig. S5). Next, to more directly address the mechanism responsible for the [Ca²⁺]_{cyt} elevation by mibefradil, we investigated the functional role of the PLC pathway using the selective PLC activator m-3M3FBS (60 μM) and the PLC inhibitor U73122 (5 μM). In the presence of 2 mM Ca²⁺ solution, m-3M3FBS elicited a significant increase in [Ca²⁺]_{cyt} in all three cell lines, with the highest increase in the Ca²⁺ peak area observed in HEK-293 cells (Fig. 4a-b). After activating PLC with m-3M3FBS, the subsequent perfusion of mibefradil (100 μM) showed only a minimal (≤ 50 nM) effect on [Ca²⁺]_{cyt} (Fig. 4c). Similarly, our data revealed that the PLC blocker U73122 (5 μM, 2 min) reduced the Δ Ca²⁺ peak in LS8 (~65%), ALC (~54%), and HEK-293 (~35%) cells (Fig. 4d-e, g-h). With the exception of the HEK-293 cells, the PLC blocker also caused a slowdown in the Ca²⁺ influx rate in LS8 and ALC cells (Fig. 4f, i). Taken together, these results support the participation of the PLC pathway and IP₃Rs in the [Ca²⁺]_{cyt} transients elicited by mibefradil.

Mibefradil triggered SOCE mediated by ORAI

Because mibefradil was able to release Ca²⁺ from ER stores and this ER-Ca²⁺ efflux is a common step in the activation of SOCE [24], we tested whether treatment with mibefradil triggers Ca²⁺ influx through SOCE. First, to exclude the possibility that plasma membrane leaks or Ca²⁺-sensing receptors (CaSRs) were associated with changes in [Ca²⁺]_{cyt}, we monitored [Ca²⁺]_{cyt} transients before and after re-addition of 2 mM extracellular Ca²⁺ in cells with replete ER-Ca²⁺ stores. We showed that this

had only a minimal effect in rising [Ca²⁺]_{cyt} (≤ 20 nM) (Fig. S6). By contrast, SOCE activation elicited by the re-addition of 2 mM Ca²⁺ in cells with ER-Ca²⁺ stores previously depleted by mibefradil resulted in a rise in [Ca²⁺]_{cyt} in all cells (~150–400 nM) (Fig. 5a-i). Next, we addressed if this SOCE effect was mediated by the ORAI channels. LS8 and ALC cells pretreated with the ORAI blocker synta-66 (5 μM, 2 h), or HEK-293 cells with a CRISPR/Cas9 deletion of *ORAI1* or HEK-293 cells lacking both *ORAI1* and *ORAI2* showed nearly abolished [Ca²⁺]_{cyt} uptake when the cells were perfused with 2 mM Ca²⁺ (Fig. 5c, f, i). These data suggest that mibefradil can elicit the activation of SOCE mediated by ORAI.

Discussion

Ca²⁺ is a key ubiquitous intracellular messenger coupling membrane-mediated processes to downstream cellular responses [32]. Therefore, Ca²⁺-mediated processes have been studied for decades in clinical and pharmacological settings [33]. Especially relevant is the use of Ca²⁺ channel antagonists (CCA), which dilate the arteries and lower blood pressure, being effective in the treatment of angina or cardiac dysrhythmias [34]. Mibefradil was launched as a new potent Ca²⁺ antagonist in 1997 to inhibit T-type (Ca_v 3.1–3.3) channels and was used in the treatment of hypertension and angina [4]. Although mibefradil was a potent and selective Ca_v 3.1–3.3 CCA at nanomolar dosage, because of its side-effects and interactions with β-blockers, it was withdrawn from the market in 1998 [35, 36]. However, because T-type (Ca_v 3.1–3.3) channels are key regulators of cancer cell proliferation and solid tumor growth [37–39], mibefradil has been recently repurposed as an anticancer drug.

Mibefradil is chemically distinct from other T-type CCA and it is 30-fold more potent against T-type Ca_v channels than L-type channels at nanomolar concentrations [4]. The anti-proliferative and anti-tumoral properties of mibefradil are in part associated with lowering AKT phosphorylation and the nuclear retention of FOX [40]. Mibefradil reduced tumor growth in resistant melanoma cells and induced apoptosis via inhibition of autophagy also activating the caspase cascade pathway [16, 41, 42]. These results suggest that the inhibition of autophagy by mibefradil might be a novel therapeutic tool

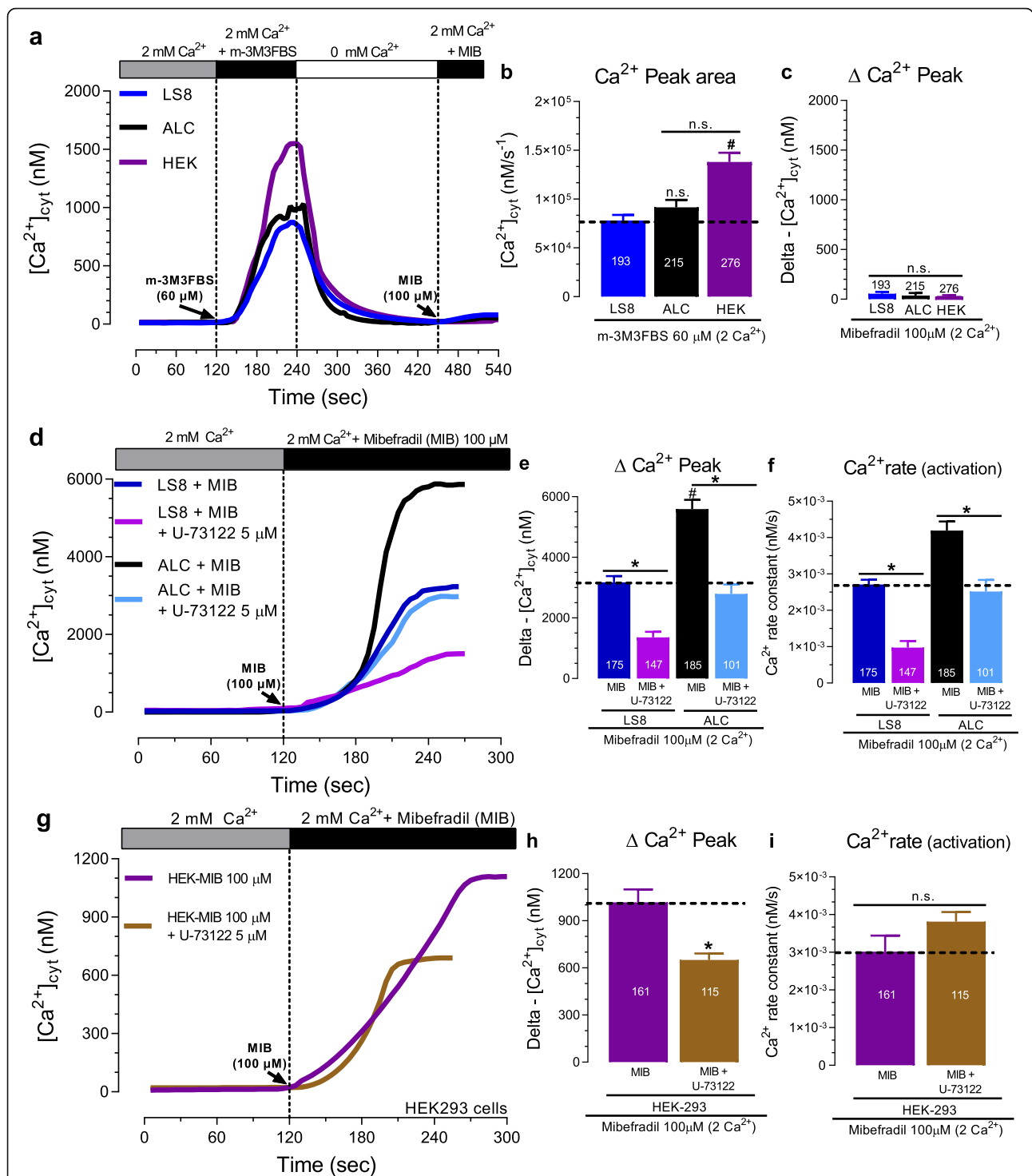


Fig. 4 Mibefradil-mediated $[Ca^{2+}]_{cyt}$ increase is dependent on PLC pathway activation. **a** Original traces of $[Ca^{2+}]_{cyt}$ transients in LS8, ALC, and HEK-293 cells stimulated with the PLC activator m-3M3FBS (60 μ M), followed by addition of mibefradil (100 μ M) in Ringer's solution containing 2 mM Ca^{2+} . **b** Quantification of the ΔCa^{2+} peak area of under m-3M3FBS stimulation. **c** Quantification of the ΔCa^{2+} peak under mibefradil stimulation. **d** Original traces of $[Ca^{2+}]_{cyt}$ transients in LS8 and ALC cells stimulated with mibefradil (100 μ M) in the presence or absence of the PLC inhibitor, U73122 (5 μ M). **e** Quantification of the ΔCa^{2+} peak. **f** Quantification of the Ca^{2+} influx rate. **g-i** Same as d-f but in HEK-293 cells. Data represent the mean \pm SEM of ≥ 101 cells from 3 independent experiments. Data were analyzed by one-way ANOVA followed by Tukey's multiple comparison post-hoc test. * $P < 0.05$ vs. LS8 group; * $P < 0.05$ vs. their respective MIB-100 μ M group; n.s., non-significant

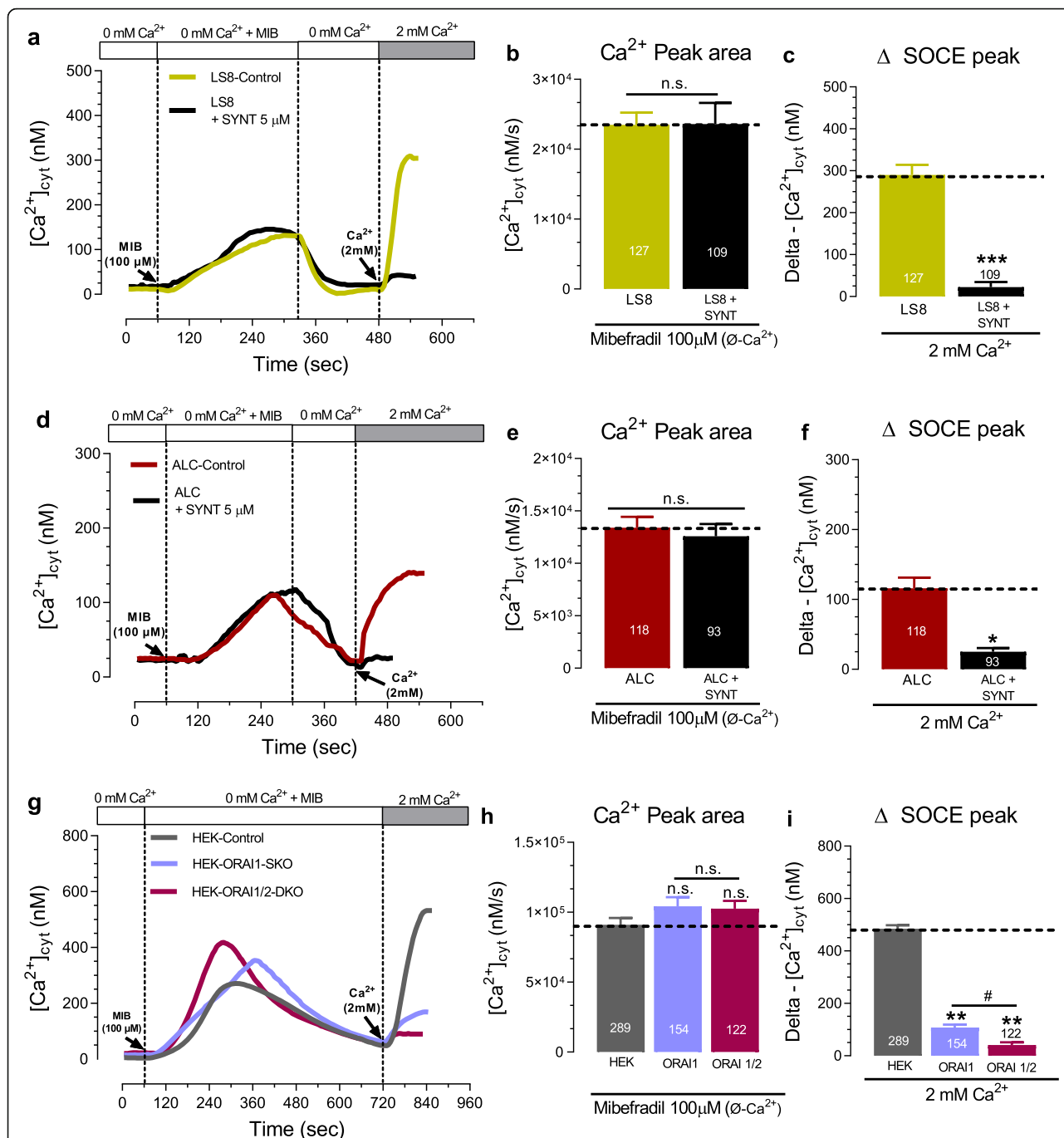


Fig. 5 Mibefradil stimulated ER-Ca²⁺ depletion and Ca²⁺ influx via SOCE. **a** Original traces of [Ca²⁺]_{cyt} transients showing ER-Ca²⁺ depletion elicited by mibefradil (100 μM) in Ca²⁺-free Ringer’s solution followed by readdition of 2 mM extracellular Ca²⁺ solution in LS8 cells with or without pre-incubation with synta-66. **b** Quantification of the ER-Ca²⁺ release peak area under mibefradil stimulation. **c** Quantification of ΔSOCE peak upon readdition of 2 mM Ca²⁺. **d** Same as in a-c but in ALC cells. **e** Same as in b-c but in ALC cells. **f** Same as in c-f but in ALC cells. **g** Original traces of [Ca²⁺]_{cyt} transients showing ER-Ca²⁺ depletion elicited by mibefradil (100 μM) in Ca²⁺-free Ringer’s solution followed by readdition of 2 mM extracellular Ca²⁺ solution in HEK-293 cells with a CRISPR-cas9 deletion of *ORAI1* (SKO) or dual deletion of *ORAI2* and *ORAI2* (DKO). **h** Quantification of the ER-Ca²⁺ release peak area under mibefradil stimulation. **i** Quantification of ΔSOCE peak upon readdition of 2 mM Ca²⁺. Data represent the mean ± SEM of ≥93 cells from 3 independent experiments. Data were analyzed by two-tailed unpaired Student’s t-test or one-way ANOVA followed by Tukey’s multiple comparison post-hoc test. **P* < 0.05 vs. ALC group; ***P* < 0.01 vs. HEK-control group; ****P* < 0.001 vs. LS8 group; #*P* < 0.05 vs. HEK-ORAI1 group; n.s., non-significant

to drive apoptosis and to reduce migration, proliferation, and tumor growth.

Although mibefradil is emerging as an anticancer drug, its pharmacokinetic profile for cancer management is not fully understood. Phase I clinical trials showed the maximum tolerated dose (MTD) by dosing 25–350 mg/day of mibefradil in four doses/day for 7–17 consecutive days [6]. This study reported that the AUC (area under the curve) of mibefradil in plasma for the final dose given on day 8 was 7797 ± 1323 ng h/mL [6], equivalent to ~ 11 – 16 μ M. Mibefradil is efficiently processed by cytochrome P450-catalysed hydrolysis and its metabolites typically represent 50–80% of the circulating drug-related compounds after a single oral dose of 100 mg [5]. Considering that our in vitro studies showed a LogEC_{50} around 45–50 μ M for mibefradil and that micromolar (≥ 10 μ M) concentrations significantly raised $[\text{Ca}^{2+}]_{\text{cyt}}$ (Fig. 1), understanding the potential cellular targets modulated by mibefradil in vitro affecting $[\text{Ca}^{2+}]_{\text{cyt}}$ should be addressed.

At micromolar concentrations, mibefradil (10 μ M) increased $[\text{Ca}^{2+}]_{\text{cyt}}$ in mammalian spermatozoa [18]. Similarly, in HEK-293, rat fibroblasts, and human platelet cells, 10 to 100 μ M of mibefradil substantially elevated $[\text{Ca}^{2+}]_{\text{cyt}}$ by unknown mechanisms [19]. Mibefradil was also reported recently to block the Ca^{2+} channel ORAI [25]. Given the limited understanding of the mechanisms by which mibefradil elevates $[\text{Ca}^{2+}]_{\text{cyt}}$, we have investigated a number of potential cellular targets and have studied their effects on Ca^{2+} uptake by SOCE mediated by the ORAI channels. We show that the transient perfusion of mibefradil elevates $[\text{Ca}^{2+}]_{\text{cyt}}$ in all cell lines tested (LS8, ALC, and HEK-293) with a concentration-dependent manner and LogEC_{50} around 45–50 μ M. Its efficiency to elevate $[\text{Ca}^{2+}]_{\text{cyt}}$ was fully reversed by perfusion of a solution without mibefradil (Fig. 1, Fig. S2).

In a wide variety of cells, the binding of agonists to transmembrane receptors triggers changes in the electrochemical driving force and can depolarize the plasma membrane increasing $[\text{Ca}^{2+}]_{\text{cyt}}$ by activation of multiple second messengers and downstream pathways [34]. One of these transmembrane receptors is the channel TRPM7 that is permeable to divalent cations (Ca^{2+} , Mg^{2+} , Mn^{2+}), and has been linked to the increase of $[\text{Ca}^{2+}]_{\text{cyt}}$ triggered by mibefradil [20, 43]. A previous report showed that mibefradil (100 μ M) increased $[\text{Ca}^{2+}]_{\text{cyt}}$ in HEK-293 cells overexpressing TRPM7 channels and that the TRPM7 antagonist NS8593 reduced the effects of mibefradil [20]. Thus, to ascertain if TRPM7 channels are a potential target of mibefradil, we stimulated the cells with the selective TRPM7 agonist naltriben. Although all cells showed the expression of

TRPM7 mRNA, the activation of TRPM7 by naltriben (100 μ M, for 5 min) in a Ringer's solution containing 2 mM Ca^{2+} only elicited a small elevation in $[\text{Ca}^{2+}]_{\text{cyt}}$ (~ 30 nM) in all cell lines (Fig. S3). These results suggest that TRPM7 channels are not the main target responsible for the changes in $[\text{Ca}^{2+}]_{\text{cyt}}$ triggered by mibefradil.

Our functional and molecular data revealed that the capacity of mibefradil to elevate $[\text{Ca}^{2+}]_{\text{cyt}}$ is associated with PLC and IP_3 signaling. We found that the transient application of mibefradil (100 μ M for 3–4 min) increased ~ 2 – 6 fold the total IP_3 content in cells (Fig. 2a–c). The binding of IP_3 to IP_3R activates the release of ER- Ca^{2+} pools. At nanomolar (500 nM) concentrations, mibefradil was reported to have no effect on the ER- Ca^{2+} , basal Ca^{2+} levels, or on the frequency of Ca^{2+} oscillations [21]. However, Eberhard et al. showed that a substantial part of the mibefradil-induced increase in $[\text{Ca}^{2+}]_{\text{cyt}}$ at micromolar concentrations (10–100 μ M) was independent of extracellular Ca^{2+} influx [19], suggesting that a potential source could be from intracellular Ca^{2+} stores. We thus tested if altering intracellular Ca^{2+} by blocking IP_3R with Xestospongine C modified the effects of mibefradil on $[\text{Ca}^{2+}]_{\text{cyt}}$. In the presence of the IP_3R inhibitor, the effects of mibefradil were markedly reduced (Fig. 3). We also showed that the prior depletion of ER- Ca^{2+} with CPA completely abolished the effects of mibefradil in $[\text{Ca}^{2+}]_{\text{cyt}}$ (Fig. 3j–l). Combined, these results suggest that the elevations in $[\text{Ca}^{2+}]_{\text{cyt}}$ induced by mibefradil are not only dependent on extracellular Ca^{2+} but also on the ER- Ca^{2+} stores. These data are in line with a previous report in rat fibroblasts and human platelets describing that mibefradil (10 μ M) caused the activation of IP_3R [19]. Our results are also consistent with reports indicating that perfusion of permeabilized cells with IP_3 prevented a rise in $[\text{Ca}^{2+}]_{\text{cyt}}$ elicited by mibefradil [19].

In non-excitable and excitable cells, the Ca^{2+} -dependent PLC pathway is essential to generate second messengers such as IP_3 and DAG that support the maintenance of $[\text{Ca}^{2+}]_{\text{cyt}}$ homeostasis [22, 23]. We showed that the main PLC isozymes (β , γ , and δ) were expressed in the three cell lines sampled (Fig. S5). We also demonstrated that, under physiological extracellular Ca^{2+} levels (2 mM Ca^{2+}), the prior activation of PLC with m-3M3FBS or inhibition of PLC with U73122, significantly reduced the effects of mibefradil (Fig. 4). Taken together, our data strongly support the role of PLC as an important mediator of the effects of mibefradil in elevating $[\text{Ca}^{2+}]_{\text{cyt}}$.

The depletion of ER- Ca^{2+} stores elicited by micromolar concentration (100 μ M) of mibefradil raised the possibility that it could also trigger Ca^{2+} influx by SOCE through ORAI channels. Our results confirmed that the increase in Ca^{2+} influx in all cell lines was mediated by

SOCE because pretreatment with the ORAI channel blocker synta-66 abolished Ca^{2+} uptake. Moreover, CRISPR/Cas9 knockdown of *ORAI1* or double deletion of *ORAI1/ORAI2* in HEK-293 cells showed that mibefradil could not elevate $[\text{Ca}^{2+}]_{\text{cyt}}$ (Fig. 5g-i). These pharmacological and molecular approaches reveal that ER- Ca^{2+} depletion elicited by mibefradil causes an increase of the $[\text{Ca}^{2+}]_{\text{cyt}}$ by Ca^{2+} influx via SOCE mediated by the ORAI channels. We suggest that this is an indirect effect on ORAI channels because mibefradil directly or indirectly activates PLC and/or IP_3 signaling.

Our data may be at odds with a previous report that mibefradil blocked the ORAI channels [25]. In overexpressing STIM1/ORAI1–3 HEK-293 cells, mibefradil (10–100 μM) blocked ORAI currents in whole-cell patch-clamp, and 24 h pretreatment with mibefradil (100 μM) abolished ER- Ca^{2+} release and SOCE [25]. By contrast, the same pretreatment using 0.1 to 50 μM of mibefradil did not interfere in the ER- Ca^{2+} or STIM1 translocation [25]. Also, 20 μM mibefradil increased $[\text{Ca}^{2+}]_{\text{cyt}}$ mediated by SOCE [26]. Reports using PHM1–41 cells showed that the acute perfusion of mibefradil at 1 μM did not change the peak of SOCE [44]. Our approach differed in that we investigated the effects of acute mibefradil perfusion, which activated SOCE. Only cells lacking functional ORAI channels could not be positively stimulated by mibefradil.

In summary, we found that mibefradil elicited a concentration-dependent increase in $[\text{Ca}^{2+}]_{\text{cyt}}$. This increase was associated with ER- Ca^{2+} release through IP_3R channels, PLC pathway activation, and triggered Ca^{2+} influx by SOCE mediated by ORAI channels. Our findings add important knowledge on the effects of mibefradil that may be of basic and clinical relevance as we provide novel targets and insights of mibefradil which should be considered in its renewed clinical use.

Materials and methods

Cell culture and genetic knockout of ORAI

The murine epithelial LS8 and ALC cell lines [45] were maintained in Dulbecco's modified Eagle's medium (DMEM) containing 10% fetal bovine serum (FBS) and 1% Penicillin-Streptomycin. All reagents were purchased from Thermo Fisher (USA). We also used HEK-293 cells, including single (*ORAI1*) and double (*ORAI1/ORAI2*) knockdowns by CRISPR/Cas9, originally reported in [46], a kind gift by Dr. Mohamed Trebak. All cells were maintained in a humidified CO_2 incubator under standard conditions (at 37 °C in a 5% CO_2), plated on 25 mm borosilicate coverslips (Fisher Scientific, USA) coated with 0.01% Poly-L-lysine (Sigma-Aldrich, USA), and used within 24 h after culture.

$[\text{Ca}^{2+}]_{\text{cyt}}$ measurements

$[\text{Ca}^{2+}]_{\text{cyt}}$ measurements were performed as previously described [28]. Briefly, cells were incubated for 1 h at room temperature with 1 μM of the ratiometric Ca^{2+} probe Fura-2-AM (Thermo Fisher, USA) in normal Ringer's solution (pH 7.4) as follows (mM): 155.0 NaCl; 4.5 KCl; 2.0 CaCl_2 ; 1.0 MgCl_2 ; 10 D-glucose; and 10 HEPES (Sigma-Aldrich, USA). Fluorescence recordings were obtained by 1) a (Nikon Ti2-E Eclipse, Japan) inverted light microscope equipped with an objective (Nikon S Fluor $\times 20$; numerical aperture: 0.75) 2) and a digital SLR camera (DS-Qi2; Nikon, Japan) controlled by computer software (NIS Elements version 5.20.01, USA). Cells were continuously perfused by a six- or eight-way perfusion system (VC-6/8 valve controller) at 5–6 ml per minute with a common outlet 0.28-mm tube driven by electrically controlled valves (Harvard Bioscience Inc., USA). A normal Ringer's solution or a Ca^{2+} -free solution (the same normal Ringer's solution, however, without 2 mM of Ca^{2+}) was used to dissolve all drugs at room temperature. Fura-2-AM was excited alternatively at 340 and 380 nm using a Lambda LS xenon-arc lamp (Sutter Instrument, USA) or pE-340 fura (Cool Led, USA). Emitted fluorescence was collected through a 510 nm emission filter. Fluorescence images were generated at 5-s intervals and the ratio values were calculated. A Fura-2 calcium imaging calibration kit (Thermo Fisher, USA) was used to estimate the $[\text{Ca}^{2+}]_{\text{cyt}}$, according to the manufacturer's specifications, as previously described [28]. Standard control buffer (background fluorescence), zero free- Ca^{2+} buffer (free- Ca^{2+}), and 39 μM free- Ca^{2+} buffer (saturating Ca^{2+}) were used to convert the emission ratio at 340/380 nm excitation to estimate the free $[\text{Ca}^{2+}]_{\text{cyt}}$.

Pharmacology and extracellular Ca^{2+} conditions

To construct mibefradil concentration-effect curves, cells were continuously perfused for 120 s in normal Ringer's solution (with regular extracellular Ca^{2+} levels, 2 mM Ca^{2+}) followed by the addition of 0.1 μM to 100 μM of mibefradil (Tocris Bioscience, USA) for 120 s. TRPM7 channel function was analyzed by perfusing the cells with the selective TRPM7-gating modulator naltriben (100 μM , Tocris Bioscience, USA) in a regular extracellular Ca^{2+} solution, as reported [28]. The effects of mibefradil on $[\text{Ca}^{2+}]_{\text{cyt}}$ were determined in normal or Ca^{2+} -free Ringer's solution supplemented with EGTA (3 mM, Sigma-Aldrich, USA). The role of IP_3R was analyzed by pretreatment with the selective IP_3R inhibitor Xestospongine C (3 μM , Tocris Bioscience, USA) for 20 min [30] prior to the application of mibefradil (100 μM). To deplete the ER- Ca^{2+} stores, cells were perfused with the reversible Ca^{2+} -ATPase (SERCA) inhibitor cyclopiazonic acid-CPA

(20 μM , Sigma-Aldrich, USA), followed by the addition of mibefradil 100 μM in Ca^{2+} -free Ringer's solution. To address the role of the PLC isoenzymes, cells were perfused with the PLC activator m-3M3FBS (60 μM) (Sigma-Aldrich, USA) as reported [47] followed by the addition of mibefradil 100 μM in regular extracellular Ca^{2+} levels (2 mM Ca^{2+}). We also use the PLC blocker U73122 (5 μM) (Sigma-Aldrich, USA) simultaneously with the application of mibefradil (100 μM) [48]. To test if mibefradil stimulates SOCE, cells were continuously perfused with mibefradil (100 μM) in Ca^{2+} -free Ringer's solution followed by a re-addition of 2 mM of extracellular Ca^{2+} in normal Ringer's solution using the CRAC blocker synta-66 (5 μM , Sigma-Aldrich, USA) for 2 h, as previously reported [28] or in HEK-293 cells with a CRISPR/Cas9 deletion of *ORAI1* or a combined *ORAI1* and *ORAI2* deletion. All drugs and chemicals were diluted and stored following the manufacturer's instructions.

Quantification of IP_3 content

IP_3 content was quantitated before and after incubation with mibefradil (100 μM , 3–4 min) using the colorimetric ELISA kit (E4792–100, BioVision incorp., USA) following the manufacturer's instructions. Briefly, 1.10^6 cells/mL were lysed and the supernatant was collected to carry out the optical density (OD) ELISA reaction assay. The IP_3 kit sensitivity is around 9 pg/mL and the concentration of IP_3 in the lysed cells can be calculated by comparing the OD of the samples to the standard curve (Fig. S7).

Real-time PCR

Total RNA was isolated using the RNeasy Micro Kit (Qiagen®), as indicated by the manufacturer, followed by reverse transcription using the iScript™ cDNA Synthesis Kit (Bio-Rad, USA). For qRT-PCR, we used the SsoAdvanced™ Universal SYBR® Green Supermix (Bio-Rad, USA) and performed the experiments in a CFX Connect thermocycler (Bio-Rad, USA) *Gapdh* was used as the housekeeping gene. Relative quantification of the gene responsible for encoding IP_3R subtype 1–3 (*ITPR1–3*) PLC β , γ , and δ (*PLCB1*, *PLCG1*, and *PLCD1*) and TRPM7 (*TRPM7*) were determined by the $2^{-\Delta\text{CT}}$ method [28]. All primers were used at 0.25 nM, and the forward/reverse sequences and amplicon size are shown in Table S1 (mouse) and Table S2 (human).

Data analyses and statistics

All data, mathematical analyses, and graphs were analyzed and/or generated using the GraphPad Prism software version 9.0 (Inc., California, USA), as previously described [28]. The ΔCa^{2+} peak and ΔSOCE peak were calculated by subtracting the maximum Ca^{2+} values from basal Ca^{2+} levels before and after pharmacological

manipulation. Ca^{2+} peak area was calculated by integrating the $[\text{Ca}^{2+}]_c$ transients versus time under the stimulus duration using Origin Pro 8 software version 8.08 (Northampton, USA). The kinetics of the rate of Ca^{2+} activation were calculated in each trace and fitted by the GraphPad Prism software using the one-phase association eq. ($Y = \text{IF}(X < X_0, Y_0, Y_0 + (\text{Plateau} - Y_0) * (1 - \exp(-K * (X - X_0))))$). Concentration-effect (0.1 μM to 100 μM) curves for mibefradil were constructed using sigmoidal log (agonist) vs. response - variable slope equation fitted by the GraphPad Prism software and parameter of the LogEC_{50} (apparent affinity) was calculated. Data represent the mean \pm SEM of the minimum of three independent experiments. The total number of cells used is indicated. Differences between the means of the group data that fit a normal distribution were analyzed using a two-tailed unpaired Student's t-test variance or by one-way ANOVA followed by Tukey's multiple comparisons post-hoc test. The limit of significance was established at * $p < 0.05$; ** $p < 0.01$; *** $p < 0.001$.

Supplementary Information

The online version contains supplementary material available at <https://doi.org/10.1186/s43556-021-00037-0>.

Additional file 1: Figure S1. Effects of Ringer's solution and mibefradil (50–100 μM) on background autofluorescence. **Figure S2.** Effects of the two consecutive mibefradil (50 μM) stimulus on $[\text{Ca}^{2+}]_{\text{cyt}}$ transients in HEK-293 cells under regular extracellular Ca^{2+} levels (2 mM Ca^{2+}). **Figure S3.** TRMP7 expression and activation by naltriben. **Figure S4.** Alternative stimulation with mibefradil (100 μM) and ATP (100 μM) under Ca^{2+} -free Ringer's solution in ALC cells. **Figure S5.** Expression of PLC isoforms. **Figure S6.** Effects of the Ca^{2+} -free Ringer's solution replacement for 2 mM extracellular Ca^{2+} in LS8, ALC, and HEK-293 cells. **Figure S7.** Optical density (OD) values of standard IP_3 concentration. **Table S1.** Mouse primers sequences for qRT-PCR used in LS8 and ALC cells. **Table S2.** Human primers sequences for qRT-PCR used in HEK-293 cells.

Acknowledgments

We thank Dr. Mohamed Trebak for kindly sharing the CRISPR/Cas9 HEK-293 cells.

Authors' contributions

GHSB and RSL designed the project; GHSB, TAF and EM performed the experiments; GHSB, EM and RSL analyzed the data; GHSB and RSL wrote the paper. All authors have approved the submitted version.

Funding

The work presented here was funded by the National Institutes for Dental and Craniofacial Research (NICDR) grants DE025639 and DE027679 to RSL.

Availability of data and materials

The data is available with the corresponding author and will be provided upon a legitimate request.

Declarations

Ethics approval and consent to participate

Not applicable.

Consent for publication

All authors consent to the publication of the data presented in this article.

Competing interests

The authors declare no conflict of interest.

Author details

¹Department of Molecular Pathobiology, New York University College of Dentistry, New York, NY 10010, USA. ²Department of Urology, New York University School of Medicine, New York, NY 10010, USA.

Received: 31 December 2020 Accepted: 24 March 2021

Published online: 30 April 2021

References

- Heady TN, Gomora JC, Macdonald TL, Perez-Reyes E. Molecular pharmacology of T-type Ca²⁺ channels. *Jpn J Pharmacol*. 2001;85(4):339–50. <https://doi.org/10.1254/jpp.85.339>.
- Strege PR, Bernard CE, Ou Y, Gibbons SJ, Farrugia G. Effect of mibefradil on sodium and calcium currents. *Am J Physiol Gastrointest Liver Physiol*. 2005;289(2):G249–53. <https://doi.org/10.1152/ajpgi.00022.2005>.
- Gómez-Lagunas F, Carrillo E, Pardo LA, Stühmer W. Gating modulation of the tumor-related Kv10.1 channel by Mibefradil. *J Cell Physiol*. 2017;232(8):2019–32. <https://doi.org/10.1002/jcp.25448>.
- Perez-Reyes E, Van Deusen AL, Vitko I. Molecular pharmacology of human Cav3.2 T-type Ca²⁺ channels: block by antihypertensives, antiarrhythmics, and their analogs. *J Pharmacol Exp Ther*. 2009;328(2):621–7. <https://doi.org/10.1124/jpet.108.145672>.
- Wiltshire HR, Sutton BM, Heeps G, Betty AM, Angus DW, Harris SR, et al. Metabolism of the calcium antagonist, mibefradil (POSICOR, Ro 40-5967). Part III. Comparative pharmacokinetics of mibefradil and its major metabolites in rat, marmoset, cynomolgus monkey and man. *Xenobiotica*. 1997;27(6):557–71. <https://doi.org/10.1080/004982597240343>.
- Holdhoff M, Ye X, Supko JG, Nabors LB, Desai AS, Walbert T, et al. Timed sequential therapy of the selective T-type calcium channel blocker mibefradil and temozolomide in patients with recurrent high-grade gliomas. *Neuro-Oncology*. 2017;19(6):845–52. <https://doi.org/10.1093/neuonc/nox020>.
- Nam G. T-type calcium channel blockers: a patent review (2012–2018). *Expert Opin Ther Pat*. 2018;28(12):883–901. <https://doi.org/10.1080/13543776.2018.1541982>.
- Barceló C, Sisó P, Maiques O, de la Rosa I, Martí RM, Macià A. T-Type Calcium Channels: A Potential Novel Target in Melanoma. *Cancers (Basel)*. 2020;12(2). DOI: <https://doi.org/10.3390/cancers12020391>
- Lijnen P, Fagard R, Petrov V. Mibefradil-induced inhibition of proliferation of human peripheral blood mononuclear cells. *J Cardiovasc Pharmacol*. 1999;33(4):595–604. <https://doi.org/10.1097/00005344-199904000-00012>.
- Schmitt R, Kleinbloesem CH, Belz GG, Schroeter V, Feifel U, Pozenel H, et al. Hemodynamic and humoral effects of the novel calcium antagonist Ro 40-5967 in patients with hypertension. *Clin Pharmacol Ther*. 1992;52(3):314–23. <https://doi.org/10.1038/clpt.1992.147>.
- Chemin J, Monteil A, Perez-Reyes E, Nargeot J, Lory P. Direct inhibition of T-type calcium channels by the endogenous cannabinoid anandamide. *EMBO J*. 2001;20(24):7033–40. <https://doi.org/10.1093/emboj/20.24.7033>.
- Hirooka K, Bertolesi GE, Kelly ME, Denovan-Wright EM, Sun X, Hamid J, et al. T-type calcium channel alpha1G and alpha1H subunits in human retinoblastoma cells and their loss after differentiation. *J Neurophysiol*. 2002;88(1):196–205. <https://doi.org/10.1152/jn.2002.88.1.196>.
- Rodrigues AL, Brescia M, Koschinski A, Moreira TH, Cameron RT, Baillie G, et al. Increase in Ca²⁺ current by sustained cAMP levels enhances proliferation rate in GH3 cells. *Life Sci*. 2018;192:144–50. <https://doi.org/10.1016/j.lfs.2017.11.040>.
- Kania E, Pająk B, Orzechowski A. Calcium homeostasis and ER stress in control of autophagy in cancer cells. *Biomed Res Int*. 2015;2015:352794. <https://doi.org/10.1155/2015/352794>.
- Wang M, Kaufman RJ. The impact of the endoplasmic reticulum protein-folding environment on cancer development. *Nat Rev Cancer*. 2014;14(9):581–97. <https://doi.org/10.1038/nrc3800>.
- Das A, Pushparaj C, Herreros J, Nager M, Vilella R, Portero M, et al. T-type calcium channel blockers inhibit autophagy and promote apoptosis of malignant melanoma cells. *Pigment Cell Melanoma Res*. 2013;26(6):874–85. <https://doi.org/10.1111/pcmr.12155>.
- Bertolesi GE, Shi C, Elbaum L, Jollimore C, Rozenberg G, Barnes S, et al. The Ca²⁺ channel antagonists mibefradil and pimozide inhibit cell growth via different cytotoxic mechanisms. *Mol Pharmacol*. 2002;62(2):210–9. <https://doi.org/10.1124/mol.62.2.210>.
- Chávez JC, De la Vega-Beltrán JL, José O, Torres P, Nishigaki T, Treviño CL, et al. Acrosomal alkalization triggers Ca²⁺ release and acrosome reaction in mammalian spermatozoa. *J Cell Physiol*. 2018;233(6):4735–47. <https://doi.org/10.1002/jcp.26262>.
- Eberhard M, Miyagawa K, Hermsmeyer K, Erne P. Effects of mibefradil on intracellular Ca²⁺ release in cultured rat cardiac fibroblasts and human platelets. *Naunyn Schmiedeberg's Arch Pharmacol*. 1995;353(1):94–101. <https://doi.org/10.1007/BF00168921>.
- Schäfer S, Ferioli S, Hofmann T, Zierler S, Gudermann T, Chubanov V. Mibefradil represents a new class of benzimidazole TRPM7 channel agonists. *Pflügers Arch*. 2016;468(4):623–34. <https://doi.org/10.1007/s00424-015-1772-7>.
- Bayguinov O, Ward SM, Kenyon JL, Sanders KM. Voltage-gated Ca²⁺ currents are necessary for slow-wave propagation in the canine gastric antrum. *Am J Physiol Cell Physiol*. 2007;293(5):C1645–59. <https://doi.org/10.1152/ajpcell.00165.2007>.
- Nakamura Y, Fukami K. Regulation and physiological functions of mammalian phospholipase C. *J Biochem*. 2017;161(4):315–21. <https://doi.org/10.1093/jb/mvw094>.
- Gressat A, Sondek J, Harden TK. The phospholipase C isozymes and their regulation. *Subcell Biochem*. 2012;58:61–94. https://doi.org/10.1007/978-94-007-3012-0_3.
- Yeung PS, Yamashita M, Prakriya M. Molecular basis of allosteric Orai1 channel activation by STIM1. *J Physiol*. 2020;598(9):1707–23. <https://doi.org/10.1113/JP276550>.
- Li P, Rubaiy HN, Chen GL, Hallett T, Zaibi N, Zeng B, et al. Mibefradil, a T-type Ca²⁺ channel blocker also blocks Orai channels by action at the extracellular surface. *Br J Pharmacol*. 2019;176(19):3845–56. <https://doi.org/10.1111/bph.14788>.
- Johnson MT, Gudlur A, Zhang X, Xin P, Emrich SM, Yeast RE, et al. L-type Ca²⁺ channel blockers promote vascular remodeling through activation of STIM proteins. *Proc Natl Acad Sci U S A*. 2020;117(29):17369–80. <https://doi.org/10.1073/pnas.2007598117>.
- Nakata A, Kameda T, Nagai H, Ikegami K, Duan Y, Terada K, et al. Establishment and characterization of a spontaneously immortalized mouse ameloblast-lineage cell line. *Biochem Biophys Res Commun*. 2003;308(4):834–9. [https://doi.org/10.1016/s0006-291x\(03\)01467-0](https://doi.org/10.1016/s0006-291x(03)01467-0).
- Souza Bomfim GH, Costinetti V, Li Y, Idaghdour Y, Lacruz RS. TRPM7 activation potentiates SOCE in enamel cells but requires ORAI. *Cell Calcium*. 2020;87:102187. <https://doi.org/10.1016/j.ceca.2020.102187>.
- Chubanov V, Mederos y Schnitzler M, Meißner M, Schäfer S, Abstiens K, Hofmann T, et al. Natural and synthetic modulators of SK (K (ca)2) potassium channels inhibit magnesium-dependent activity of the kinase-coupled cation channel TRPM7. *Br J Pharmacol*. 2012;166(4):1357–1376. DOI: <https://doi.org/10.1111/j.1476-5381.2012.01855.x>.
- Ozaki H, Hori M, Kim YS, Kwon SC, Ahn DS, Nakazawa H, et al. Inhibitory mechanism of xestospongine-C on contraction and ion channels in the intestinal smooth muscle. *Br J Pharmacol*. 2002;137(8):1207–12. <https://doi.org/10.1038/sj.bjp.0704988>.
- Dadsetan S, Zakharova L, Molinski TF, Fomina AF. Store-operated Ca²⁺ influx causes Ca²⁺ release from the intracellular Ca²⁺ channels that is required for T cell activation. *J Biol Chem*. 2008;283(18):12512–9. <https://doi.org/10.1074/jbc.M709330200>.
- Parys JB, Bultynck G. Calcium signaling in health, disease and therapy. *Biochim Biophys Acta Mol Cell Res*. 2018;1865(11 Pt B):1657–9. <https://doi.org/10.1016/j.bbamcr.2018.08.019>.
- Islam MS. Calcium signaling: from basic to bedside. *Adv Exp Med Biol* 2020; 1131:1–6. DOI: https://doi.org/10.1007/978-3-030-12457-1_1.
- Elliott WJ, Ram CV. Calcium channel blockers. *J Clin Hypertens (Greenwich)*. 2011;13(9):687–9. <https://doi.org/10.1111/j.1751-7176.2011.00513.x>.
- Po AL, Zhang WY. What lessons can be learnt from withdrawal of mibefradil from the market? *Lancet*. 1998;351(9119):1829–30. [https://doi.org/10.1016/s0140-6736\(05\)78800-0](https://doi.org/10.1016/s0140-6736(05)78800-0).
- Mullins ME, Horowitz BZ, Linden DH, Smith GW, Norton RL, Stump J. Life-threatening interaction of mibefradil and beta-blockers with dihydropyridine calcium channel blockers. *Jama*. 1998;280(2):157–8. <https://doi.org/10.1001/jama.280.2.157>.
- Krouse AJ, Gray L, Macdonald T, McCray J. Repurposing and rescuing of Mibefradil, an antihypertensive, for Cancer: a case study. *Assay Drug Dev Technol*. 2015;13(10):650–3. <https://doi.org/10.1089/adt.2015.29014.ajkdr>.

38. Gray LS, Perez-Reyes E, Gomora JC, Haverstick DM, Shattock M, McLatchie L, et al. The role of voltage gated T-type Ca²⁺ channel isoforms in mediating "capacitative" Ca²⁺ entry in cancer cells. *Cell Calcium*. 2004;36(6):489–97. <https://doi.org/10.1016/j.ceca.2004.05.001>.
39. Gray LS, Schiff D, Macdonald TL. A model for the regulation of T-type Ca (2+) channels in proliferation: roles in stem cells and cancer. *Expert Rev Anticancer Ther*. 2013;13(5):589–95. <https://doi.org/10.1586/era.13.34>.
40. Dziegielewska B, Casarez EV, Yang WZ, Gray LS, Dziegielewski J, Slack-Davis JK. T-type Ca²⁺ channel inhibition sensitizes ovarian Cancer to carboplatin. *Mol Cancer Ther*. 2016;15(3):460–70. <https://doi.org/10.1158/1535-7163.MCT-15-0456>.
41. Maiques O, Barceló C, Panosa A, Pijuan J, Orgaz JL, Rodriguez-Hernandez I, et al. T-type calcium channels drive migration/invasion in BRAFV600E melanoma cells through Snail1. *Pigment Cell Melanoma Res*. 2018;31(4):484–95. <https://doi.org/10.1111/pcmr.12690>.
42. Maiques O, Macià A, Moreno S, Barceló C, Santacana M, Veà A, et al. Immunohistochemical analysis of T-type calcium channels in acquired melanocytic naevi and melanoma. *Br J Dermatol*. 2017;176(5):1247–58. <https://doi.org/10.1111/bjd.15121>.
43. Chubanov V, Ferioli S, Gudermann T. Assessment of TRPM7 functions by drug-like small molecules. *Cell Calcium*. 2017;67:166–73. <https://doi.org/10.1016/j.ceca.2017.03.004>.
44. Murtazina DA, Chung D, Ulloa A, Bryan E, Galan HL, Sanborn BM. TRPC1, STIM1, and ORAI influence signal-regulated intracellular and endoplasmic reticulum calcium dynamics in human myometrial cells. *Biol Reprod*. 2011;85(2):315–26. <https://doi.org/10.1095/biolreprod.111.091082>.
45. Sarkar J, Simanian EJ, Tuggy SY, Bartlett JD, Snead ML, Sugiyama T, et al. Comparison of two mouse ameloblast-like cell lines for enamel-specific gene expression. *Front Physiol*. 2014;5:277. <https://doi.org/10.3389/fphys.2014.00277>.
46. Yoast RE, Emrich SM, Zhang X, Xin P, Johnson MT, Fike AJ, et al. The native ORAI channel trio underlies the diversity of Ca (2+) signaling events. *Nat Commun*. 2020;11(1):2444. <https://doi.org/10.1038/s41467-020-16232-6>.
47. Chi CC, Chou CT, Kuo CC, Hsieh YD, Liang WZ, Tseng LL, et al. Effect of m-3m3FBS on Ca²⁺ handling and viability in OC2 human oral cancer cells. *Acta Physiol Hung*. 2012;99(1):74–86. <https://doi.org/10.1556/APhysiol.99.2012.1.8>.
48. Use of U-73122 as an Inhibitor of Phospholipase C-Dependent Processes. *Neuroprotocols*. 1993;3(2):125–33. DOI: <https://doi.org/10.1006/ncmn.1993.1046>

Publisher's Note

Springer Nature remains neutral with regard to jurisdictional claims in published maps and institutional affiliations.